HHS Public Access

Author manuscript

J Control Release. Author manuscript; available in PMC 2021 May 28.

Published in final edited form as:

J Control Release. 2021 January 10; 329: 762–773. doi:10.1016/j.jconrel.2020.10.010.

Microsphere antioxidant and sustained erythropoietin-R76E release functions cooperate to reduce traumatic optic neuropathy

C.R. DeJulius[a,1], **A. Bernardo-Colón**[b,1], **S. Naguib**[c], **J.R. Backstrom**[a,b], **T. Kavanaugh**[a], **M.K. Gupta**[a], **C.L. Duvall**[a,*], **T.S. Rex**[b,c,*]

[a]Department of Biomedical Engineering, Vanderbilt University, United States

[b]Vanderbilt Eye Institute, Vanderbilt University Medical Center, United States

[c]Department of Ophthalmology & Visual Science, Vanderbilt University School of Medicine, United States

Abstract

Wild-type erythropoietin (EPO) is promising for neuroprotection, but its therapeutic use is limited because it causes a systemic rise in hematocrit. We have developed an EPO-R76E derivative that maintains neuroprotective function without effects on hematocrit, but this protein has a short half-life *in vivo.* Here, we compare the efficacy and carrier-induced inflammatory response of two polymeric microparticle (MP) EPO-R76E sustained release formulations based on conventional hydrolytically degradable poly(lactic-*co*-glycolic acid) (PLGA) and reactive oxygen species (ROS)-degradable poly(propylene sulfide) (PPS). Both MP types effectively loaded EPO-R76E and achieved sustained release, providing detectable levels of EPO-R76E at the injection site in the eye *in vivo* for at least 28 days. Testing in an *in vitro* oxidative stress assay and a mouse model of blast-induced indirect traumatic optic neuropathy (bITON) showed that PPS and PLGA MP-mediated delivery of EPO-R76E provided therapeutic protection. While unloaded PLGA MPs inherently increase levels of pro-inflammatory cytokines in the bITON model, drug-free PPS MPs have innate antioxidant properties that provide therapeutic benefit both *in vitro* and *in vivo.* Both PLGA and PPS MPs enabled sustained release of EPO-R76E, providing therapeutic benefits including reduction in inflammation and axon degeneration, and preservation of visual function as measured by electroretinogram. The PPS-based MP platform is especially promising for further development, as the delivery system provides inherent antioxidant benefits that can be harnessed to work in complement with EPO-R76E or other drugs for neuroprotection in the setting of traumatic eye injury.

[*]Corresponding authors at: Department of Biomedical Engineering, Vanderbilt University, and Vanderbilt Eye Institute, Vanderbilt University Medical Center, United States. craig.duvall@vanderbilt.edu (C.L. Duvall), tonia.rex@vumc.org (T.S. Rex).

[1]These authors contributed equally.

Appendix A. Supplementary data

Supplementary data to this article can be found online at https://doi.org/10.1016/j.jconrel.2020.10.010.

Keywords

Antioxidant; Microparticle; Intraocular; Neurotrauma; Neuroprotection; Sustained delivery; Erythropoietin

1. Introduction

There is a need for better neuroprotective therapeutics for treatment of complex neurodegenerative processes lacking a defined genetic target, such as neurotrauma. Traumatic brain injuries occur in 2.8 million civilians each year [1], and indirect traumatic optic neuropathy (ITON) is estimated to occur in 0.5% to 2% of these individuals [2]. The natural history of ITON is not well understood due to the low incidence of the condition and the high variability of its course in patients [3,4]. Animal studies and case reports suggest that the neurodegeneration and loss of vision stabilizes about 1-month after injury [5–7]. Notably, current interventions for ITON are no more effective than observation alone [8]. Unlike treatment of inherited conditions, it may not be advantageous, or even safe, to provide permanent and irreversible treatment (*e.g.,* with a viral gene therapy) with a neuroprotective agent, as these agents are often pleiotropic. However, other types of local treatments may require frequent re-injection into the eye due to short-lasting effects (*e.g.,* weekly), which increases the risk of hemorrhage, elevated intraocular pressure, retinal detachment, endophthalmitis, and inflammation [9–13]. Thus, it is desirable to provide sustained, but not permanent, treatment with tight dose control. A major reason for the short duration of injected therapeutics is the clearance mechanisms of the intravitreal space, including conjunctival, choroidal, and lymphatic circulation [14], motivating use of controlled-release systems that respond to environmental cues to trigger matrix degradation and cargo release [15]. For example, drug-releasing ocular implants have been investigated for treatment of various conditions. Ozurdex and Durysta are two such implants, composed of poly(lactic-*co*-glycolic acid) (PLGA) and delivering Dexamethasone and Bimatoprost, respectively [16,17]. In addition to bulk implants, injectable, micron-sized (~1–100 μm) particles are large enough to provide size-based retention of therapeutics in the intravitreal space [18] and extend the benefit of ocular drugs.

We and others have previously demonstrated that erythropoietin (EPO) can preserve retinal neurons and optic nerve axons in a variety of models of neuronal cell death including our model of blast-induced ITON (bITON) [6,7,19]. Recently, microparticle (MP)-mediated delivery of EPO for nerve regeneration has gained interest. Rong and colleagues formulated a dextran-EPO poly(lactic-*co*-glycolic acid)/poly (lactic acid) (PLGA/PLA) MP system and demonstrated its efficacy in a rat model of optic nerve crush. A single injection of their MP system significantly rescued retinal ganglion cells (RGCs) 4 and 8 weeks post-optic nerve crush; to achieve the same effect with free EPO, injections were required every 2 weeks [20]. Similarly, Zhang and colleagues showed that a single local injection of PLGA-EPO MPs significantly increased nerve conduction velocity, muscle action potentials, axon counts, and myelin thickness in a rat sciatic nerve defect model 8 weeks post-surgery [21]. These results demonstrate the ability of PLGA MPs to improve EPO efficacy by providing slow release of the drug.

In this study, we compare the therapeutic efficacy of a mutant EPO (EPO-R76E) delivered intraocularly by two different polymeric MP systems in a model of bITON. EPO-R76E carries a mutation that converts the arginine at position 76 to a glutamate. This mutation prevents the significant and potentially dangerous increase in hematocrit caused by systemic administration of wild-type EPO in non-anemic animals, while preserving equal neuroprotective efficacy [22,23]. We compare EPO-R76E formulated into MPs comprising the clinical gold standard PLGA or poly(propylene sulfide) (PPS). PPS is a hydrophobic polymer that transitions to hydrophilic upon oxidation by ROS such as hydrogen peroxide (H_2O_2) [24]. We previously showed that PPS MMPs undergo ROS-triggered drug cargo release and that the inherent PPS reactivity with ROS can provide therapeutically-relevant antioxidant benefits (in the absence of a drug) for treatment of peripheral arterial disease and mechanical load-induced osteoarthritis [25,26].

Because elevated ROS cause oxidative stress that exacerbates inflammatory disorders, including neurodegenerative diseases [25–27], we sought to test whether the ROS scavenging behavior of PPS would contribute therapeutic neuroprotection in the setting of bITON. By contrast, PLGA degrades *via* nonspecific hydrolysis into acidic byproducts which lower the local pH [28], which can worsen inflammation upon subcutaneous implantation [29]. Notably, oxidative stress is a central hallmark of our bITON model, causing secondary axon degeneration [6]. Thus, we hypothesized that ROS-responsive, EPO-R76E-loaded PPS MPs could provide sustained local release of EPO-R76E within the eye and that both components of the MPs (PPS and EPO-R76E) could positively contribute to the neuroprotective function of the formulation.

2. Methods

2.1. EPO-R76E purification

Human epithelial kidney (HEK) cells grown to confluence in 10 cm plates were transfected with 5 μg of mammalian expression plasmids (pcDNA3.1(+), Thermo Fisher, cat #V790-20, Waltham, MA) that express either wild-type EPO or EPO-R76E with carboxyl-terminal His-tags. A 19-amino acid linker containing a Tobacco Etch Virus (TEV) protease recognition site was inserted after the carboxyl-terminus of EPO-R76E to increase the accessibility of the His-tag to the metal ion matrix used for purification. The next day, plates were washed and replaced with serum-free DMEM. After an additional three days, the media was collected and centrifuged to pellet cells. Supernatant was applied to a TALON cobalt resin column (Takara BIO, Mountain View, CA) and washed with 20 bed volumes of phosphate buffered saline (PBS). Protein was eluted from the matrix with 50 mM potassium acetate, pH 5.0 buffer containing 100 mM NaCl. The pH of the solution was neutralized with a 1:40 volume (2.5 μ100 μl eluate) of 0.8 M Tris, pH 9.3. Protein was judged to be at least 90% pure based on gels stained with SimplyBlue SafeStain (Invitrogen, Carlsbad, CA). His-tagged EPO or EPO-R76E was detected on blots with mouse anti-His tag (Cell Signaling, Danvers MA; #2366 diluted 1:1000) or rabbit anti-hEPO (R&D Systems Inc., Minneapolis MN; #AB286 at 1 μg/ml).

2.2. Synthesis of PPS

PPS was prepared by anionic polymerization of propylene sulfide (Sigma-Aldrich, St. Louis, MO) using 1,8-diazabicyclo[5.4.0]undec-7-ene (DBU)/1-butane thiol as an initiator [30–32]. Briefly, DBU (4.5 mmol, 0.673 ml) and anhydrous tetrahydrofuran (THF, 10 ml) were transferred to a dried 25 ml round bottom (RB) flask and degassed for 30 min. In another 50 ml RB flask, 1-butane thiol (1.5 mmol, 0.161 ml) in THF (20 ml) was degassed for 30 min, and the reaction mixture temperature was lowered to 0 °C. To this solution, the previously degassed solution of DBU in THF was added dropwise. The flask was brought to room temperature and allowed to stir for 30 min. Next, freshly distilled and degassed propylene sulfide (120 mmol, 9.39 ml) monomer was added dropwise to the reaction mixture at 0 °C and maintained for 30 min. After 2 h stirring at room temperature, the polymerization reaction was quenched by addition of 2-iodoethanol (2 mmol, 0.40 g) and stirred overnight at room temperature. The next day, the polymer solution was filtered to remove precipitated salt and further purified by three precipitations into cold methanol before vacuum-drying to yield a colorless viscous polymer. PPS chemical structure was confirmed *via* ^{1}H NMR recorded in deuterated chloroform ($CDCl_3$) with a Brüker 400 MHz spectrometer. ^{1}H NMR (400 MHz; $CDCl_3$, δ): 1.3–1.4 (s, CH_3), 2.5–2.8 (s, CH), 2.8–3.1 (s, CH_2), 3.72 (t, CH_2-OH). (poly(PPS), Mn = 6700 g/mol, PDI = 1.3).

2.3. Characterization of PPS

PPS was characterized for structure, molecular weight (Mn), and polydispersity (PDI) as described previously [25,26,30–32]. Gel permeation chromatography (GPC, Agilent Technologies, Santa Clara, CA, USA) was used to assess Mn and PDI of the polymer. PPS was dissolved in dimethylformamide (DMF) + 0.1 M LiBr and run through three serial Tosoh Biosciences TSKGel Alpha columns (Tokyo, Japan) at 60 °C. Offline injections into the Agilent refractive index (RI) detector were performed to determine the polymer dn/dc value. The dn/dc value was used to calculate absolute Mn using the RI detector and a Wyatt miniDAWN TREOS light scattering (LS) detector (Wyatt Technology Corp., Santa Barbara, CA).

2.4. EPO-R76E microparticle formulation

PPS or PLGA (10 kDa, 50:50 lactide:glycolide, Sigma) was dissolved in dichloromethane (DCM) at 50 mg/ml (100 mg polymer in 2 ml DCM). For EPO-R76E-loaded MPs, 500 μl EPO-R76E (470 μg/ml) was added dropwise, and the mixture was homogenized at 20,000 rpm for 30 s. The mass ratio of polymer:EPO-R76E was 425:1; this relatively high ratio was used to ensure a sufficient dose of PPS was given to leverage its antioxidant function. The resulting polymer solution was added dropwise to 1.5% polyvinyl alcohol (PVA, 10 ml), and this mixture was homogenized at 10,000 rpm for 30 s. To remove DCM, the MP suspension underwent rotary evaporation for 1 h. The MPs were washed once with deionized (DI) water to remove excess PVA and resuspended in DI water. The suspension was frozen at −80 °C and lyophilized until further use. Unloaded MPs were formulated similarly without the addition of EPO-R76E.

2.5. Quantification of EPO-R76E loading

EPO-R76E was labeled with N-hydroxysuccinimide-cyanine7 (NHS-Cy7) dye to quantify protein loading into PPS and PLGA MPs. Briefly, 500 μl sodium bicarbonate buffer (0.3 M, pH 8.3) was added to 1 ml EPO-R76E (250 μg/ml). NHS-Cy7 was dissolved in dimethyl sulfoxide (DMSO) at 589 μM, and 100 μl was added to the EPO-R76E solution (final concentration 36.8 μM). The mixture was reacted at room temperature for 4 h on a shaker. The EPO-R76E-Cy7 protein was purified *via* a desalting column. The fluorescently-labeled protein was lyophilized to yield a dry powder. The protein yield was measured by bicinchoninic acid (BCA) assay. EPO-R76E-Cy7-loaded MPs were formulated as above. The MPs were fully dissolved in DMSO, and the fluorescence of the released EPO-R76E was measured on a plate reader at excitation/emission 750/773 nm. EPO-R76E concentration was calculated from a standard curve of EPO-R76E-Cy7 in DMSO.

2.6. Optical microscopy

PLGA, PLGA+EPO-R76E, PPS, and PPS + EPO-R76E MPs were resuspended in DI water. A 50 μl droplet was placed on a coverslip and allowed to settle for 30 min. Five images per sample were acquired on a Nikon Eclipse Ti inverted microscope. MP size was measured using Nikon Ts software. One hundred MPs per image were measured.

2.7. Dynamic light scattering

Dynamic light scattering (DLS) was used to quantify the size distribution of MPs (Zetasizer Nano ZA, Malvern Instruments, Westborough, MA). MP samples were resuspended at 1 mg/ml in 1 × PBS and transferred to 1 ml plastic cuvettes for measurement.

2.8. Scanning electron microscopy

Scanning electron microscopy (SEM) was used to investigate morphology of MPs (Zeiss Merlin SEM, GEMINI II column). MPs were resuspended in DI water and a droplet was added to a piece of conductive tape attached to a SEM stub. The water was evaporated overnight, and the MPs were sputter coated with gold for 70 s (Cressington Sputter Coater) before imaging.

2.9. Quantification of microparticle endotoxin levels

Endotoxin levels were quantified using the commercially available ToxinSensor™ Chromogenic LAL Endotoxin Assay Kit (GenScript) according to the manufacturer's protocol. Briefly, 0.4 mg microparticles (MPs) in 100 μl endotoxin-free PBS were combined with 100 μl reconstituted Limulus Amebocyte Lysate (LAL) and incubated at 37 °C for 10 min. 100 μl chromogenic substrate was added, incubated for 6 min. This was followed by addition of 500 μl stop solution and 1 ml color stabilizer. Each sample was plated in triplicate (100 μl per well) in a black-walled 96-well plate, and the absorbance was read at 545 nm on a plate reader. The endotoxin levels were quantified from a standard curve.

2.10. In Vitro release of EPO-R76E

PLGA+EPO-R76E or PPS + EPO-R76E MPs were resuspended in PBS at 4 mg/ml. 250 μl of suspension was added to a 12-well plate transwell submerged in 1 ml PBS, 50 mM H_2O_2,

or 500 mM H_2O_2. These H_2O_2 concentrations were chosen because they have been shown to induce ARPE-19 cell death [33]. The well plate was agitated throughout the course of the study on a plate shaker at 37 °C. The releasate was collected over time, and replaced with fresh PBS or H_2O_2 solution, and frozen at −80 °C until EPO-R76E quantification.

2.11. EPO-R76E ELISA

EPO-R76E concentration in the releasates was measured by sandwich ELISA using a Quantikine Human EPO ELISA kit (R&D Systems, Minneapolis, MN) according to manufacturer directions. Samples were loaded at 10 μl per well and tested in duplicate, and the results were averaged.

2.12. Cell culture

The human retinal pigment epithelial ARPE-19 cell lines obtained from the American Type Culture Collection (ATCC, Manassas, VA; #CRL-2302) were grown in DMEM/F12 Medium (Gibco #10565–018) with 10% fetal bovine serum (FBS; Gibco # 26140–079) and 15 mM HEPES buffer (Gibco #15630–080). The cells were maintained in a standard incubator at 37 °C and 5% CO_2.

2.13. Microparticle cytotoxicity assay

ARPE-19 cells were seeded in 96-well plates in serum-free medium and allowed to adhere for 24 h. The media was replaced with 100 μl media containing MP suspensions at varying concentrations. The doses were calculated to deliver 10, 20, 40, or 80 ng EPO-R76E, or a corresponding dose of unloaded MPs (0.08, 0.16, 0.32, or 0.64 mg/ml PLGA MPs; 0.1, 0.2, 0.4, or 0.8 mg/ml PPS MPs). After 24 h, cell viability was measured using the Cell TiterGlo kit according to the manufacturer's protocol: 100 μl Cell TiterGlo reagent was added to each well, and the luminescence was measured on an *In Vivo* Imaging System (IVIS).

2.14. Protection from H_2O_2 in vitro

Cytoprotection of the MPs from H_2O_2-induced death was measured *via* trypan blue stain. ARPE-19 cells were treated with 300 μM H_2O_2 to induce cell death [33] and with MPs comprising PLGA, PLGA+EPO-R76E, PPS, or PPS + EPO-R76E (50 ng EPO-R76E). After 24 h, cells were collected and stained with trypan blue, and cell death was quantified using a hemocytometer.

2.15. Quantification of intracellular of ROS

Intracellular ROS was measured using dihydroethidium (DHE; ThermoFisher Scientific, Waltham, MA). ARPE-19 cells were treated with 100 μM H_2O_2 alone or with PLGA, PLGA +EPO-R76E, PPS, or PPS + EPO-R76E (50 ng EPO-R76E). After 6 h, cells were washed twice with HBSS and loaded with 10 μM DHE. After cells were incubated for 30 min, dye was removed, and cells were washed and analyzed on a fluorescence plate reader (POLARstar Omega, BMG Labtech Company) at 581 nm emission, 608 nm emission.

2.16. bITON model

Eye injury was induced as previously described [6,19]. All experiments were performed in the morning. Briefly, C57Bl/6 J mice (Jackson Labs, Bar Harbor, ME) were anesthetized with 1.5% isofluorane and secured into a padded housing chamber. The housing chamber was placed inside of a pipe. The left eye of the mouse was positioned against a hole in the pipe, which was aligned with the barrel of a paintball marker. Mice were exposed to two 15 psi air-blasts at a 0.5 s interval per day for three days. Sham mice were anesthetized and placed in the trauma system, but the air was blocked from reaching the eye. Mice were provided gel recovery food (Clear H_2O, Portland, ME) for the first 3-days post-injury. At 1-day after the last blast exposure, mice were anesthetized with isofluorane and injected with a single 1 μl intravitreal injection using a 30 gauge Hamilton syringe. Mice were injected with PBS, PPS with or without EPO-R76E (at 10 μg MP/μl PBS), or PLGA with or without EPO-R76E (at 10 μg MP/μl PBS). EPO-R76E levels in the eye were quantified *via* ELISA as described above after sonicating the tissue in 2 ml PBS + Halt 100 × protease inhibitor cocktail (25 μl) and 10% Triton X-100 (50 μl). All experiments were conducted in compliance with the ARVO Statement for the Use of Animals in Ophthalmic and Vision Research. This study was carried out under an animal protocol approved by the Vanderbilt University Medical Center Institutional Animal Care and Use Committee.

2.17. In vivo ROS imaging

Mice were anesthetized with isofluorane and intravitreally injected with 1 μl of DHE in PBS using a 30-gauge Hamilton syringe. Just prior to imaging, mice were anesthetized with 20/8/0.8 mg/kg ketamine/xylazine/urethane, and eyes were dilated with tropicamide. 30 min after DHE injection, fluorescence was imaged on a Micron IV retinal imaging microscope (Phoenix Research Labs, Pleasanton, CA) using an FF02-475/50 nm excitation filter (Semrock, Inc. Rochester, NY) and ET620/60× emission filter (Chroma Technology Corp., Bellows Falls, VT). Using ImageJ software, the average intensity of the fluorescence throughout the retina was quantified. Mice were imaged at 4 weeks after injury, just prior to euthanasia and tissue collection.

2.18. SOD2 western blot

Single retinas were homogenized, sonicated in lysis buffer, and centrifuged. Sample buffer was added to the supernatant just prior to use. Known amounts of superoxide dismutase 2 (SOD2) protein (10 to 20 μg) or protein ladder were loaded into each well of an SDS-poly-acrylamide gel. The Bio-Rad mini-trans blot cell system and mini protean pre-cast gels at 4–20% were used (Hercules, CA). Loading control was HSP60 (rabbit; 1:1000; ab45134, Abcam, Cambridge, MA). The protein was transferred onto nitrocellulose using the Bio-Rad trans blot turbo transfer system (Hercules, CA), probed with anti-SOD2 (rabbit; 1:1000; ab13533; Abcam), probed with secondary antibody (alkaline phosphatase-conjugated AffiniPure Goat Anti-Rabbit IgG; 1:1000; cat #133466; Jackson ImmunoResearch Laboratories), and detected with alkaline phosphatase substrate. Band density was quantified by scanning the blot using an EPSON scanner and Adobe Photoshop to convert to grayscale and invert the image. Each band was selected with the same frame, and set measurements were used to obtain the grey mean value for each.

2.19. Multiplex cytokine ELISA

A mouse multiplex cytokine/chemokine magnetic bead panel (cat #: MCYTOMAG-70 K, Millipore, Burlington, MA) for interleukin-1α (IL-1α) and IL-1β was performed according to manufacturer directions. Samples were tested in duplicate and results were averaged.

2.20. Histological assessment of optic nerve

Optic nerve was post-fixed in glutaraldehyde followed by embedding in Resin 812 and Araldite 502 (cat # 14900 and 10900, Electron Microscopy sciences, Hatfield, PA) according to a previously published protocol [6,7,19,34]. A Leica EM-UC7 microtome was used to collect 1 μm-thick sections. Sections were then stained with 1% para-phenylenediamine and 1% toluidine blue and were imaged on a Nikon Eclipse Ni-E microscope using a 100× oil immersion objective (Nikon Instruments Inc., Melville, NY). Both total and degenerating axons were quantified using ImageJ software. A grid was used to count 20% of the optic nerve cross-sectional area to avoid bias.

2.21. Electroretinograms (ERG) and Visual Evoked Potentials (VEPs)

Mice were dark-adapted overnight, dilated with 1% tropicamide for 10 min, and anesthetized with 20/8/0.8 mg/kg ketamine/xylaxine/urethane according to previously published methodology [6,7,34]. Mice were placed on the heated surface of the ERG system to maintain body temperature. Corneal electrodes with integrated stimulators were placed on eyes lubricated with Genteel drops using the Celeris system (Diagnosys LLC, Lowell, MA). Subdermal platinum needle electrodes were placed in the snout and back of the head at the location of the visual cortex. A ground electrode was placed in the back of the mouse. For scotopic VEPs, mice were exposed to 50 flashes of 1 Hz, 0.5 cd.s/m^2 white light. To collect scotopic ERGs, electrodes were placed on lubricated corneas. Mice were then exposed to 15 flashes of 1 Hz, 1 cd.s/m^2.

2.22. Experimental design and statistical analysis

Western blot data was normalized to loading controls. Data were analyzed using GraphPad Prism (La Jolla, CA). All experimental groups were compared to each other using a one-way ANOVA and the Tukey post-hoc test. All groups are shown as mean ± standard deviation with the exception of the cytokine levels, which are shown as standard error (SE) in order to adjust the y-axis as needed for comparison purposes.

3. Results and discussion

3.1. Formulation of EPO-R76E-loaded microparticles

We and others have shown a dangerous rise in hematocrit with systemic administration of EPO [22,23,35], which we avoided here by using mutant EPO-R76E and intravitreal administration. EPO and EPO-R76E with a carboxyl-terminal His-tag (Fig. 1A, top) were expressed in mammalian HEK cells, rather than bacterial cells, in order to properly glycosylate the proteins. Our initial attempt to purify proteins from culture supernatant resulted in low levels of recovered wild-type EPO and no detectable EPO-R76E (Fig. 1B lanes 1 and 2, respectively). This was due to the His-tag being mostly inaccessible for

purification rather than a lack of protein expression (data not shown). Therefore, a 15-amino acid tobacco etch virus (TEV) peptide was used as a spacer between the EPO proteins and His-tag to increase accessibility of the His tag (Fig. 1A, bottom). This approach enhanced recovery of purified wild-type EPO or EPO-R76E from culture supernatants (Fig. 1B lanes 3 and 4, respectively). As further confirmation, we probed blots with anti-EPO (Fig. 1C) and compared our purified proteins (lanes 2 and 3) to commercially available EPO (lanes 4–6). The purified proteins and purchased EPO were detected by the EPO antibody and migrated at similar sizes. The EPO-R76E-TEV-His-tagged protein was used in all following experiments and is henceforth referred to as EPO-R76E.

To extend the residence time of EPO-R76E in the eye, EPO-R76E was loaded into PPS and PLGA MPs using the W/O/W emulsion technique. PPS was synthesized by anionic polymerization and characterized by ^{1}H NMR and GPC (Fig. 1D–F). In order to determine the amount of EPO-R76E loaded into the PPS and PLGA MPs, the protein was labeled with Cy7 and quantified from a standard curve (Fig. 1G). PPS and PLGA MPs were loaded with 0.85 and 1.39 μg EPO-R76E per mg MPs, respectively. Though this loading amount is relatively low (~0.1 wt%), the potency of EPO-R76E is such that relatively low protein levels are neuroprotective. Though the high polymer quantity per loaded protein cargo may be a concern for PLGA, the PPS polymer has inherent antioxidant properties that we seek to leverage as a complement to the bioactivity of EPO-R76E.

Blank and loaded MPs were quantified for size by light microscopy and DLS. A representative image of unloaded PPS MPs is shown in Fig. 1H. Quantification shows that the PLGA MPs were slightly larger than the PPS MPs (Fig. 1I–L and Supplemental Fig. 1); all MPs were in the range of 1–5 μm (Table 1). EPO-R76E loaded MPs tended to be slightly smaller than their unloaded counterparts. This size difference between loaded and unloaded MPs is not anticipated to be functionally significant but could be due to differences in the particle fabrication process. The process for creating the blank (protein free) particles did not include a primary W/O emulsion and instead utilized a simpler O/W emulsion process whereby polymer dissolved in DCM was homogenized directly into an aqueous PVA solution prior to DCM evaporation and particle hardening. Additional MP analysis by optical microscopy and SEM revealed spherical particles with a smooth surface with the exception of the PLGA+EPO-R76E group (Supplemental Fig. 2). This group exhibited a more irregular surface morphology, possibly due to the rotary evaporation step that was utilized at the end of the W/O/W emulsion process, a step that enabled more reproducible production of stable, homogeneous particles for the PPS MPs.

3.2. In vitro efficacy of EPO-R76E microparticles

We compared release of EPO-R76E over time from the PPS and PLGA MPs *in vitro* (Fig 2A, B). Because PPS is sensitive to ROS, we tested release in two different concentrations of hydrogen peroxide (H_2O_2), as well as PBS (Fig. 2A). The PPS MPs released EPO-R76E at a similar rate to PLGA in PBS, likely by a diffusion-controlled release mechanism. However, the rate of release from PPS MPs was accelerated in a dose-dependent fashion by addition of H_2O_2. Under all conditions, the PPS MPs showed an initial burst followed by a relatively

constant, sustained release profile. Overall, both PPS and PLGA demonstrated sustained release of EPO-R76E in PBS for at least 3 weeks *in vitro.*

Next, we assessed the cytocompatibility of different doses of empty or EPO-R76E-loaded MPs (Fig. 2C). Although some statistically significant differences were detected between groups, all groups exhibited greater than 90% viability when treated with 10–80 ng EPO-R76E in 10–80 μg PPS or 8–64 μg PLGA MPs. For the remaining *in vitro* experiments, we treated cells with 50 ng EPO-R76E delivered in either 40 μg PLGA or 50 μg PPS MPs based on pilot dose-finding studies.

To demonstrate the benefit of the inherently antioxidant PPS delivery system and to decouple the antioxidant effects of PPS from those of EPO-R76E, *in vitro* cytoprotection and intracellular ROS levels were measured under oxidative conditions. First, we exposed cells to 300 μM H_2O_2 and co-treated with either empty or EPO-R76E-loaded PPS or PLGA MPs (Fig. 2D). After 24 h, there was 38 ± 2.5% and 36 ± 6.0% cell death in the untreated and empty PLGA treated groups, respectively. In contrast, only 13 ± 2%, 12 ± 3%, and 9 ± 3% cell death was detected in the PLGA+EPO-R76E, PPS alone, and PPS + EPO-R76E treated groups, respectively ($p < 0.0001$ *vs.* untreated). Therefore, any mode of EPO-R76E delivery rescued cells from ROS-induced cell death whereas PLGA alone failed to have any benefit. In contrast, there was a significant cell protective benefit of PPS alone in the presence of a large dose of H_2O_2, confirming the inherent antioxidant, cell-protective activity of PPS. This result is in agreement with previous data showing that unloaded PPS MPs can prevent cell death at levels similar to PPS MPs loaded with the antioxidant and anti-inflammatory compound curcumin [26].

We next quantified the level of intracellular ROS in ARPE-19 cells after exposure to 100 μM H_2O_2 for 6 h using DHE fluorescence (Fig. 2E, F). All data were normalized to the level of DHE fluorescence in naïve cells (media) and are shown as percent increase from the control group. Empty PPS MPs significantly decreased DHE fluorescence, and this effect was compounded with the addition of EPO-R76E, returning ROS levels to baseline (Fig. 2E). The cellular ROS scavenging ability of PPS-based micro- and nanoparticles has been demonstrated previously in cell types including RAW264.7 macrophages, 3T3 fibroblasts, primary human mesenchymal stem cells (hMSCs), and BV2 microglial cells, agreeing with our results [26,31,32,36]. PLGA-mediated delivery of EPO-R76E also suppressed DHE fluorescence to control levels, with no effect from empty PLGA MPs (Fig 2F). These data demonstrate that EPO-R76E can decrease ROS beyond that accomplished by PPS alone with moderate exposure to H_2O_2, and to our knowledge, are the first demonstration of the combined antioxidant effect of PPS MPs and EPO-R76E.

3.3. In vivo efficacy of EPO-R76E microparticles

To study the long-term benefits of EPO-R76E MPs, we utilized the bITON model in which there is elevated ROS that contributes to secondary degeneration of the optic nerve [6]. For *in vivo* experiments, the polymer mass was controlled to directly compare the effects of PPS *vs.* PLGA. The total calculated dose of MP encapsulated EPO-R76E injected into the eye was 1.01 and 1.65 U/eye for PPS and PLGA, respectively. First, we assessed the persistence of EPO-R76E in the eye after injection of the MPs 1-day after the last blast exposure (Fig.

3). Low levels of endogenous EPO were present in the empty PPS (Fig. 3A) or PLGA-(Fig. 3B) injected eyes at both 3- and 28-days post-injection. Both PPS and PLGA MPs facilitated the persistence of EPO-R76E over 28 days in the vitreous (Fig. 3A–B), indicating a controlled-release profile.

Since PPS MPs degrade in the presence of elevated H_2O_2 and hypochlorite [25,26], we anticipated that the release of EPO-R76E from PPS MPs is at least partially controlled by injury-associated production of ROS. In line with this expectation and with our *in vitro* release studies, which showed a higher burst release in the presence of H_2O_2, we saw a higher amount of EPO-R76E in the PPS MP eyes on day 1 than the latter timepoints. Conversely, PLGA created a relatively constant level of EPO-R76E in the eye at day 1 relative to the remainder of the timecourse. The higher initial release from PPS MPs is thought to be associated with “on demand” release due to the oxidative burst that occurs acutely following ON injury [37], whereas PLGA is inert to this environmental stimulus. This on-demand release may better protect the eye by creating a higher concentration of available EPO-R76E during the critical stage immediately following injury. Following this initial burst release of the protein at the first timepoint, the amount of EPO-R76E was lower but consistently present at about 20 mU/mL over the remainder of the timepoints out to 28 days. These results suggest that both MP formulations significantly extend the persistence of EPO-R76E in the eye, releasing measurable protein quantities into the eye for at least one month. In contrast, we have previously shown that the concentration of free EPO in the eye decreases 1000-fold by 36 h after intra-ocular injection in mice [38], and a study in rabbits found a half-life of intravitreal EPO to be 2.84 days [39]. Notably, the average concentration of EPO-R76E in the eye over the 5 time points post-injection was 0.11 mU/eye and 0.16 mU/eye for PPS and PLGA MPs, respectively, based on assuming a volume of 5.3 μl/mouse eye. This estimated EPO-R76E concentration in the eye falls within a range that we have previously shown to be neuroprotective (0.06–0.32 mU/eye) [38,40–42].

To investigate the antioxidant effect of sustained EPO-R76E *in vivo,* we quantified DHE fluorescence in the retina 4 weeks after bITON in mice treated with PLGA or PLGA+EPO-R76E. This experiment focused on the PLGA MPs so that we could better identify any potential side effects of the PLGA-based MPs and also isolate the effect of the EPO-R76E protein without the complicating factor of using the ROS-scavenging PPS MPs (Fig. 4A–C). A higher DHE signal was present in the retina of bITON eyes injected with empty PLGA MPs (Fig. 4A) than in those treated with PLGA+EPO-R76E (Fig. 4B). Quantification of the fluorescence showed a reduction to near sham levels in the PLGA+EPO-R76E eyes ($p < 0.01$ as compared to PLGA alone; Fig. 4C), demonstrating that EPO-R76E can reduce the ROS burst induced by bITON, while unloaded PLGA MPs have no effect on ROS levels.

We hypothesize that the major mechanistic difference between the antioxidant effects of PPS and EPO-R76E is that EPO-R76E can activate gene expression of antioxidant proteins whereas PPS directly reacts with and scavenges ROS. To test the gene expression effects, we quantified levels of SOD2 (a mitochondria-associated enzyme that detoxifies superoxide free radicals) in the retina (Fig 4D, E). We have previously shown that levels of ROS-protective SOD2 decrease dramatically after blast injury [6]. We also have shown in a glaucoma model that systemic virus-mediated EPO-R76E gene delivery can increase expression of

antioxidant proteins in the retina [43]. Here, we also show a decrease in retinal SOD2 levels in saline-injected bITON animals and in bITON mice injected with either the PPS or PLGA MPs alone (Fig. 4E). Notably, while both unloaded MP types exhibited SOD2 reduction, SOD2 levels in the retina were significantly higher with PPS treatment than PLGA. These data suggest that ROS scavenging by the PPS MPs may have mitigated the loss of SOD2. Treatment with EPO-R76E-loaded PPS or PLGA MPs was even more effective at preventing the loss of SOD2. The rescue of SOD2 levels in both groups of EPO-R76E treated retinas suggests that EPO-R76E and PPS have different antioxidant mechanisms that would be anticipated to have collaborative, beneficial effects on reducing ROS-mediated TON.

Our trauma model causes an increase in ROS followed by an increase in levels of the pro-inflammatory cytokines IL-1α and IL-1β [6]. Further, blocking ROS prior to and after injury prevents increases in these cytokines and reduces secondary axon degeneration and vision loss [6]. Therefore, we quantified changes in the levels of IL-1α and IL-1β in both the retina and optic nerve (Fig. 4F–I). Levels of inflammatory cytokines were higher in the retina and optic nerve from bITON eyes injected with PLGA MPs alone compared to those receiving saline injection (Fig. 4F–I). We measured endotoxin levels in the MPs to ensure that the increase in cytokine levels was not due to endotoxin contamination; as expected, endotoxin levels were low (Supplemental Fig. 3). Therefore, we expect this additional increase in inflammatory cytokines is due to some facet of either the physical properties or the acidic degradation products of PLGA MPs. The inflammatory effects of intraocular PLGA MPs have been observed by others [44]; modifications of the MPs such as a hydrophilic PEG coating have been shown to reduce this inflammation [44,45]. In contrast, the antioxidant effects of PPS alone, PPS + EPO-R76E, and PLGA+EPO-R76E prevented increases in both cytokines after bITON. This result is consistent with our previous observations using a prophylactic antioxidant diet [6]; the major difference is that in the current study, the MPs were given at 1-day after injury, a more clinically relevant treatment protocol. These data highlight the inherent benefit of using PPS for MP-based, local drug delivery in neurodegenerative applications, as the carrier contributes significantly to neuroprotection by suppressing levels of major pathological cytokines.

To investigate tissue damage, we assessed the optic nerve histologically 4 weeks after injury under all treatment conditions (Fig. 5). Sham optic nerves showed a high density of axons with clear axoplasms and tight myelin sheaths, along with normal morphology of astrocytes (Fig. 5A). In contrast, the bITON optic nerves had axons with loose or collapsed myelin and hypertrophic astrocytes (Fig. 5B). The optic nerves from eyes injected with the empty PPS MPs appeared to have a high density of axons, although some degenerative profiles and glial hypertrophy were still evident (Fig. 5C). The optic nerves from eyes injected with PPS + EPO-R76E or PLGA+EPO-R76E displayed a morphology similar to sham (Fig 5D, F). In contrast, degenerative axon profiles were evident in the optic nerves of bITON mice injected with PLGA alone (Fig. 5E). Quantification of total axons showed a significant loss of axons in the bITON mice injected with saline or PLGA; however, PPS, PPS + EPO-R76E, and PLGA+EPO-R76E all had axon counts similar to sham (Fig. 5G). This illustrates the protective effects of either empty PPS or the EPO-R76E-loaded MPs. As expected, there was an increase in degenerative axon profiles in the bITON mice as compared to shams, and PLGA MP treatment further worsened axon degeneration, $p < 0.001$ as compared to bITON

saline (Fig 5H). This is likely explained by the elevation in the pro-inflammatory cytokines IL-1α and IL-1β (Fig. 4F–I). In contrast, there was no difference in degenerative axon profiles between shams and the EPO-R76E loaded PPS or PLGA MP-injected groups (Fig. 5H). The PPS alone group showed an intermediate effect, again demonstrating the protective effect of PPS. These data further suggest that the antioxidant activity of PPS provides a therapeutic benefit in this ROS-driven pathology, whereas PLGA demonstrated no therapeutic benefit and possibly exacerbated inflammation as demonstrated by cytokine levels (Fig 4F–I).

We next assessed if post-injury delivery of the EPO-R76E loaded PPS or PLGA MPs could preserve visual function (Fig. 6). Representative ERG waveforms show the a- and b-waves 4 weeks after blast injury in the saline and PPS groups (Fig. 6A). Our injury paradigm causes a reduction in the ERG b-wave amplitude and an increase in the latency, indicative of synaptic dysfunction at the level of the retinal bipolar cells (Fig. 6B,C) [34]. Treatment with unloaded PLGA MPs had no effect on b-wave amplitude (b_{max}) or latency. Unloaded PPS-treated eyes trended towards improved b_{max} and showed a significant improvement in the b-wave latency compared to bITON saline. Loading with EPO-R76E in both PPS and PLGA MPs significantly improved both the ERG b_{max} and latency compared to bITON saline (Fig. 6B,C). Blast injury also causes a reduction in the VEP N1 amplitude and an increase in the N1 latency, indicative of damage to the optic nerve [6,7]. Representative VEP waveforms from the saline and PPS groups are shown Fig. 6D. The N1 amplitude and latency were significantly improved by treatment with empty PPS MPs, but not with empty PLGA MPs (Fig. 6E,F). Loading with EPO-R76E into either PPS or PLGA MPs yielded improvement in both N1 amplitude and latency (Fig. 6E,F).

The combined ERG data suggest that controlled release of EPO-R76E protects visual function in the bITON model and that the PPS MP carrier alone can also contribute to functional protection in this injury model. We anticipate that EPO-R76E delivery with PPS MPs has potential to outperform delivery with PLGA MPs either with lower EPO-R76E dose in the bTON model or in more aggressive disease or injury models. However, for the formulation and dosing regimes tested in the current study, both of the EPO-R76E controlled release MP groups were, in most cases, not statistically different from the baseline sham groups, complicating our ability to detect any added benefit of the PPS relative to PLGA MPs in the context of sustained EPO-R76E release.

It will be of interest, based on our previous studies [38,40], to explore how relative quantity of PPS to EPO-R76E affects efficacy and whether increased relative loading of EPO-R76E will yield better outcomes for more complex or long-term neurodegeneration such as glaucoma. The potential clinical significance of this study is further supported by our use of a relevant disease treatment scenario where treatment was given one day after three consecutive days of blast injury. Notably, molecular injury processes are initiated in this model prior to the last day of blast exposure [19], suggesting a wider therapeutic window for the treatment of secondary neurodegeneration due to neurotrauma than previously thought.

4. Conclusions

Here, we compared PLGA- and PPS-based MPs for sustained release of EPO-R76E in a bITON model of traumatic neuropathy utilizing a clinically relevant treatment paradigm. Both PLGA and PPS MPs effectively loaded EPO-R76E and provided sustained release for at least a month *in vivo.* Drug-free PLGA MPs showed no benefit in neuroprotection and in fact exacerbated cytokine production associated with the bITON model. However, both PPS and PLGA MPs loaded with EPO-R76E provided robust therapeutic benefit, strongly indicating the therapeutic value of EPO-R76E sustained release. In contrast to PLGA, drug-free PPS MPs, which react irreversibly with some ROS, provided partial protection against the mechanical injury and consequent induction of inflammation and axon degeneration. These results extend our previous findings that ROS are causative of axon degeneration and vision loss in the bITON model. The combined results of this study further confirm the neuroprotective effects of EPO-R76E and suggest that PPS-based MPs are a promising carrier worthy of further development for sustained therapeutic delivery in models of neurodegeneration.

Supplementary Material

Refer to Web version on PubMed Central for supplementary material.

Acknowledgements

The authors thank Purnima Ghose for assistance with histology and microscopy and the VAPR Core for assistance in purification of Histagged EPO-R76E. In addition, they thank the Vanderbilt Institute for Nanoscale Science and Engineering (VINSE) for use of the DLS and SEM instruments. The syringe and mouse graphics were obtained from Servier Medical Art.

Funding

This work was supported by DoD W81XWH-15-1-0096 (TR), DoD W81XWH-17-2-0055 (TR), NEI R01 EY022349 (TR, CD), NEI U24 EY029893 (TR), NIBIB T32-EB021937 (CD), NIA R01 NS094595 (TR), Potocsnak Discovery Grant in Regenerative Medicine (TR), Ayers Foundation Regenerative Visual Neuroscience Pilot Grant (TR), Ret. Maj. General Stephen L. Jones, MD Fund (TR), Vanderbilt University Medical Center Cell Imaging Shared Resource core facility (Clinical and Translational Science Award Grant UL1 RR024975 from National Center for Research Resources), NEI P30EY008126 (VVRC), T32 EY021833 (VVRC) and Research Prevent Blindness, Inc. (VEI). The funding sources had no involvement in the study design, or collection, analysis, or interpretation of the data. The authors confirm that there are no known conflicts of interest associated with this publication and there has been no significant financial support for this work that could have influenced its outcome.

References

[1]. Taylor CA, Bell JM, Breiding MJ, Xu L, Traumatic brain injury-related emergency department visits, hospitalizations, and deaths — United States, 2007 and 2013, Morb. Mortal. Wkly. Rep. Surveill. Summ 66 (2017) 1–16, 10.15585/mmwr.ss6609a1.

[2]. Steinsapir KD, Goldberg RA, Traumatic optic neuropathy, Surv. Ophthalmol. 38 (1994) 487–518, 10.1016/0039-6257(94)90145-7. [PubMed: 8066541]

[3]. Steinsapir KD, Goldberg RA, Traumatic optic neuropathy: an evolving understanding, Am J. Ophthalmol. 151 (2011) 928–933, 10.10l6/j.ajo.2011.02.007. [PubMed: 21529765]

[4]. Singman EL, Daphalapurkar N, White H, Nguyen TD, Panghat L, Chang J, McCulley T, Indirect traumatic optic neuropathy, Mil. Med. Res. 3 (2016) 2, 10.1186/s40779-016-0069-2. [PubMed: 26759722]

[5]. Miliaras G, Fotakopoulos G, Asproudis I, Voulgaris S, Zikou A, Polyzoidis K, Indirect traumatic optic neuropathy following head injury: report of five patients and review of the literature, J. Neurol. Surg. A Cent. Eur. Neurosurg. 74 (2013) 168–174, 10.1055/s-0032-1330115. [PubMed: 23397127]

[6]. Bernardo-Colón A, Vest V, Clark A, Cooper ML, Calkins DJ, Harrison FE, Rex TS, Antioxidants prevent inflammation and preserve the optic projection and visual function in experimental neurotrauma, Cell Death Dis. 9 (2018) 1097, 10.1038/s41419-018-1061-4. [PubMed: 30367086]

[7]. Bernardo-Colôn A, Vest V, Cooper ML, Naguib SA, Calkins DJ, Rex TS, Progression and pathology of traumatic optic neuropathy from repeated primary blast exposure, Front. Neurosci 13 (2019) 719, 10.3389/fnins.2019.00719. [PubMed: 31354422]

[8]. Levin LA, Beck RW, Joseph MP, Seiff S, Kraker R, The treatment of traumatic optic neuropathy: the international optic nerve trauma study, Ophthalmol 106 (1999) 1268–1277, 10.1016/S0161-6420(99)00707-1.

[9]. Daniel E, Toth CA, Grunwald JE, Jaffe GJ, Martin DF, Fine SL, Huang J, Ying GS, Hagstrom SA, Winter K, Maguire MG, Risk of scar in the comparison of age-related macular degeneration treatments trials, Ophthalmol 121 (2014) 656–666, 10.1016/j.ophtha.2013.10.019.

[10]. Day S, Acquah K, Mruthyunjaya P, Grossman DS, Lee PP, Sloan FA, Ocular complications after anti-vascular endothelial growth factor therapy in Medicare patients with age-related macular degeneration, Am J. Ophthalmol. 152 (2011) 266–272, 10.1016/j.ajo.2011.01.053. [PubMed: 21664593]

[11]. Sharma S, Johnson D, Abouammoh M, Hollands S, Brissette A, Rate of serious adverse effects in a series of bevacizumab and ranibizumab injections, Can. J. Ophthalmol. 47 (2012) 275–279, 10.1016/j.jcjo.2012.03.026. [PubMed: 22687306]

[12]. Pershing S, Bakri SJ, Moshfeghi DM, Ocular hypertension and intraocular pressure asymmetry after intravitreal injection of anti-vascular endothelial growth factor agents, Ophthal. Surg. Lasers Imaging Retina 44 (2013) 460–464, 10.3928/23258160-20130909-07.

[13]. Gregori NZ, Flynn HW Jr., Schwartz SG, Rosenfeld PJ, Vaziri K, Moshfeghi AA, Fortun JA, Kovach JL, Dubovy SR, Albini TA, Davis JL, Berrocal AM, Smiddy WE, Current infectious endophthalmitis rates after intravitreal injections of anti-vascular endothelial growth factor agents and outcomes of treatment, Ophthal. Surg. Lasers Imaging Retina 46 (2015) 643–648, 10.3928/23258160-20150610-08.

[14]. Gaudana R, Ananthula HK, Parenky A, Mitra AK, Ocular drug delivery, AAPS J. 12 (2010) 348–360, 10.1208/sl2248-010-9183-3. [PubMed: 20437123]

[15]. Sahil K, Akanksha M, Premjeet S, Bilandi A, Kapoor B, Microsphere: a review, Int. J. Res. Pharm. Chem 1 (2011) 1184–1198.

[16]. Bansal R, Bansal P, Kulkarni P, Gupta V, Sharma A, Gupta A, Wandering Ozurdex® implant, J. Ophthal. Inflamm. Infect. 2 (2012) 1–5, 10.1007/s12348-011-0042-x.

[17]. Shirley M, Bimatoprost implant: first approval, Drugs Aging 37 (2020) 457–462, 10.1007/s40266-020-00769-8. [PubMed: 32447639]

[18]. Shelke NB, Kadam R, Tyagi P, Rao VR, Kompella UB, Intravitreal poly(L-lactide) microparticles sustain retinal and choroidal delivery of TG-0054, a hydrophilic drug intended for neovascular diseases, Drug Deliv. Transl. Res. 1 (2010) 76–90, 10.1007/sl3346-010-0009-8.

[19]. Vest V, Bernardo-Colón A, Watkins D, Kim B, Rex TS, Rapid repeat exposure to subthreshold trauma causes synergistic axonal damage and functional deficits in the visual pathway in a mouse model, J. Neurotrauma 36 (2019) 1646–1654, 10.1089/neu.2018.6046. [PubMed: 30451083]

[20]. Rong X, Yang S, Miao H, Guo T, Wang Z, Shi W, Mo X, Yuana W, Jin T, Effects of erythropoietin-dextran microparticle-based PLGA/PLA microspheres on RGCs, Investig. Ophthalmol. Vis. Sci. 53 (2012) 6025–6034, 10.1167/iovs.12-9898. [PubMed: 22871834]

[21]. Zhang W, Zhou G, Gao Y, Zhou Y, Liu J, Zhang L, Long A, Zhang L, Tang P, A sequential delivery system employing the synergism of EPO and NGF promotes sciatic nerve repair, Colloids Surf. B 159 (2017) 327–336, 10.1016/j.colsurfb.2017.07.088.

[22]. Sullivan T, Kodali K, Rex TS, Systemic gene delivery protects the photoreceptors in the retinal degeneration slow mouse, Neurochem. Res. 36 (2011) 613–618, 10.1007/s11064-010-0272-6. [PubMed: 20924671]

[23]. Sullivan TA, Geisert EE, Hines-Beard J, Rex TS, Systemic adeno-associated virus-mediated gene therapy preserves retinal ganglion cells and visual function in DBA/2J glaucomatous mice, Hum. Gene Ther. 22 (2011) 1191–1200, 10.1089/hum.2011.052. [PubMed: 21542676]

[24]. Napoli A, Valentini M, Tirelli N, Muller M, Hubbell JA, Oxidation-responsive polymeric vesicles, Nat. Mater. 3 (2004) 183–189, 10.1038/nmatl081. [PubMed: 14991021]

[25]. O'Grady KP, Kavanaugh TE, Cho H, Ye H, Gupta MK, Madonna MC, Lee J, O'Brien CM, Skala MC, Hasty KA, Duvall CL, Drug-free ROS sponge polymeric microspheres reduce tissue damage from ischemic and mechanical injury, ACS Biomater. Sci. Eng. 4 (2018) 1251–1264, 10.1021/acsbiomaterials.6b00804. [PubMed: 30349873]

[26]. Poole KM, Nelson CE, Joshi RV, Martin JR, Gupta MK, Haws SC, Kavanaugh TE, Skala MC, Duvall CL, ROS-responsive microspheres for on demand antioxidant therapy in a model of diabetic peripheral arterial disease, Biomaterials 41 (2015) 166–175, 10.1016/j.biomaterials.2014.ll.016. [PubMed: 25522975]

[27]. Lisanti MP, Martinez-Outschoorn UE, Lin Z, Pavlides S, Whitaker-Menezes D, Pestell RG, Howell A, Sotgia F, Hydrogen peroxide fuels aging, inflammation, cancer metabolism and metastasis, Cell Cycle 10 (2011) 2440–2449, 10.4161/cc.10.15.16870. [PubMed: 21734470]

[28]. Zolnik BS, Burgess DJ, Effect of acidic pH on PLGA microsphere degradation and release, J. Control. Release 122 (2007) 338–344, 10.1016/j.jconrel.2007.05.034. [PubMed: 17644208]

[29]. Ji W, Yang F, Seyednejad H, Chen Z, Hennink WE, Anderson JM, van den Beucken JJ, Jansen JA, Biocompatibility and degradation characteristics of PLGA-based electrospun nanofibrous scaffolds with nanoapatite incorporation, Biomaterials 33 (2012) 6604–6614, 10.1016/j.biomaterials.2012.06.018. [PubMed: 22770568]

[30]. Gupta MK, Martin JR, Dollinger BR, Hattaway ME, Duvall CL, Thermogelling ABC Triblock copolymer platform for resorbable hydrogels with tunable, degradation-mediated drug release, Adv. Funct. Mater. 27 (2017) 1704107, 10.1002/adfm.201704107. [PubMed: 30349427]

[31]. Gupta MK, Martin JR, Werfel TA, Shen T, Page JM, Duvall CL, Cell protective ABC Triblock polymer-based thermoresponsive hydrogels with ROS-triggered degradation and drug release, J. Am. Chem. Soc. 136 (2014) 14896–14902, 10.1021/ja507626y. [PubMed: 25254509]

[32]. Dollinger BR, Gupta MK, Martin JR, Duvall CL, Reactive oxygen species shielding hydrogel for the delivery of adherent and nonadherent therapeutic cell types, Tissue Eng. Part A 23 (19–20) (2017), 10.1089/ten.tea.2016.0495.

[33]. Yang P, Peairs JJ, Tano R, Jaffe GJ, Oxidant-mediated Akt activation in human RPE cells, Investig. Ophthalmol. Vis. Sci. 47 (2006) 4598–4606, 10.1167/iovs.06-0140. [PubMed: 17003457]

[34]. Naguib S, Bernardo-Colon A, Cencer C, Gandra N, Rex TS, Galantamine protects against synaptic, axonal, and vision deficits in experimental neurotrauma, Neurobiol. Dis. 134 (2019) 104695, 10.1016/j.nbd.2019.104695. [PubMed: 31778813]

[35]. Tripathy SK, Svensson EC, Black HB, Goldwasser E, Margalith M, Hobart PM, Leiden JM, Long-term expression of erythropoietin in the systemic circulation of mice after intramuscular injection of a plasmid DNA vector, Proc. Natl. Acad. Sci. U. S. A. 93 (1996) 10876–10880, 10.1073/pnas.93.20.10876. [PubMed: 8855275]

[36]. Rajkovic O, Gourmel C, d'Arcy R, Wong R, Rajkovic I, Tirelli N, Pinteaux E, Reactive oxygen species-responsive nanoparticles for the treatment of ischemic stroke, Adv. Ther 2 (2019) 7, 10.1002/adtp.201900038.

[37]. O'Hare Doig RL, Bartlett CA, Maghzal GJ, Lam M, Archer M, Stocker R, Fitzgerald M, Reactive species and oxidative stress in optic nerve vulnerable to secondary degeneration, Exp. Neurol. 261 (2014) 136–146, 10.1016/j.expneurol.2014.06.007. [PubMed: 24931225]

[38]. Rex TS, Wong Y, Kodali K, Merry S, Neuroprotection of photoreceptors by direct delivery of erythropoietin to the retina of the retinal degeneration slow mouse, Exp. Eye Res. 89 (2009) 735–740, 10.1016/j.exer.2009.06.017. [PubMed: 19591826]

[39]. Zhang J, Wu Y, Xu J, Ye W, Xhang Y, Weng H, Shi W, Xu G, Lu L, Dai W, Sinclair SH, Li W, Xu G, Pharmacokinetic and toxicity study of intravitreal erythropoietin in rabbits, Acta Pharmacol. Sin. 29 (2008) 1383–1390, 10.1111/j.1745-7254.2008.00885.x. [PubMed: 18954534]

[40]. Hines-Beard J, Desai S, Haag R, Esumi N, D'Surney L, Parker S, Richardson C, Rex TS, Identification of a therapeutic dose of continuously delivered erythropoietin in the eye using an inducible promoter system, Curr. Gene Ther. 13 (2013) 275–281, 10.2174/15665232113139990024. [PubMed: 23773177]

[41]. Rex TS, Allocea M, Domenici L, Surace EM, Maguire AM, Lyubarsky A, Cellerino A, Bennett J, Auricchio A, Systemic but not intraocular EPO gene transfer protects the retina from light- and genetic-induced degeneration, Mol. Ther. 10 (2004) 855–861, 10.1016/j.ymthe.2004.07.027. [PubMed: 15509503]

[42]. Rex TS, Kasmala L, Bone WS, de Lucas Cerrillo AM, Wynn K, Lewin AS, Erythropoietin slows photoreceptor cell death in a mouse model of autosomal dominant retinitis Pigmentosa, PLoS One 14 (2016) e0157411.

[43]. Hines-Beard J, Bond WS, Backstrom JR, Rex TS, Virus-mediated EpoR76E gene therapy preserves vision in a glaucoma model by modulating neuroinflammation and decreasing oxidative stress, J. Neuroinflammation 13 (2016) 39, 10.1186/s12974-016-0499-5. [PubMed: 26876380]

[44]. McDonnell PJ, Khan YA, Lai SK, Kashiwabuchi RT, Behrens A, Hanes JS, Sustained Delivery of Therapeutic Agents to an Eye Compartment, (2019) (US10369107B2).

[45]. Tsujinaka H, Fu J, Shen J, Yu Y, Hafiz Z, Kays J, McKenzie D, Cardona D, Culp D, Peterson W, Gilger BC, Crean CS, Zhang J, Kanan Y, Yu W, Cleland JL, Yang M, Hanes J, Campochiaro PA, Sustained treatment of retinal vascular diseases with self-aggregating sunitinib microparticles, Nat. Commun 11 (2020) 694, 10.1038/s41467-020-14340-x. [PubMed: 32019921]

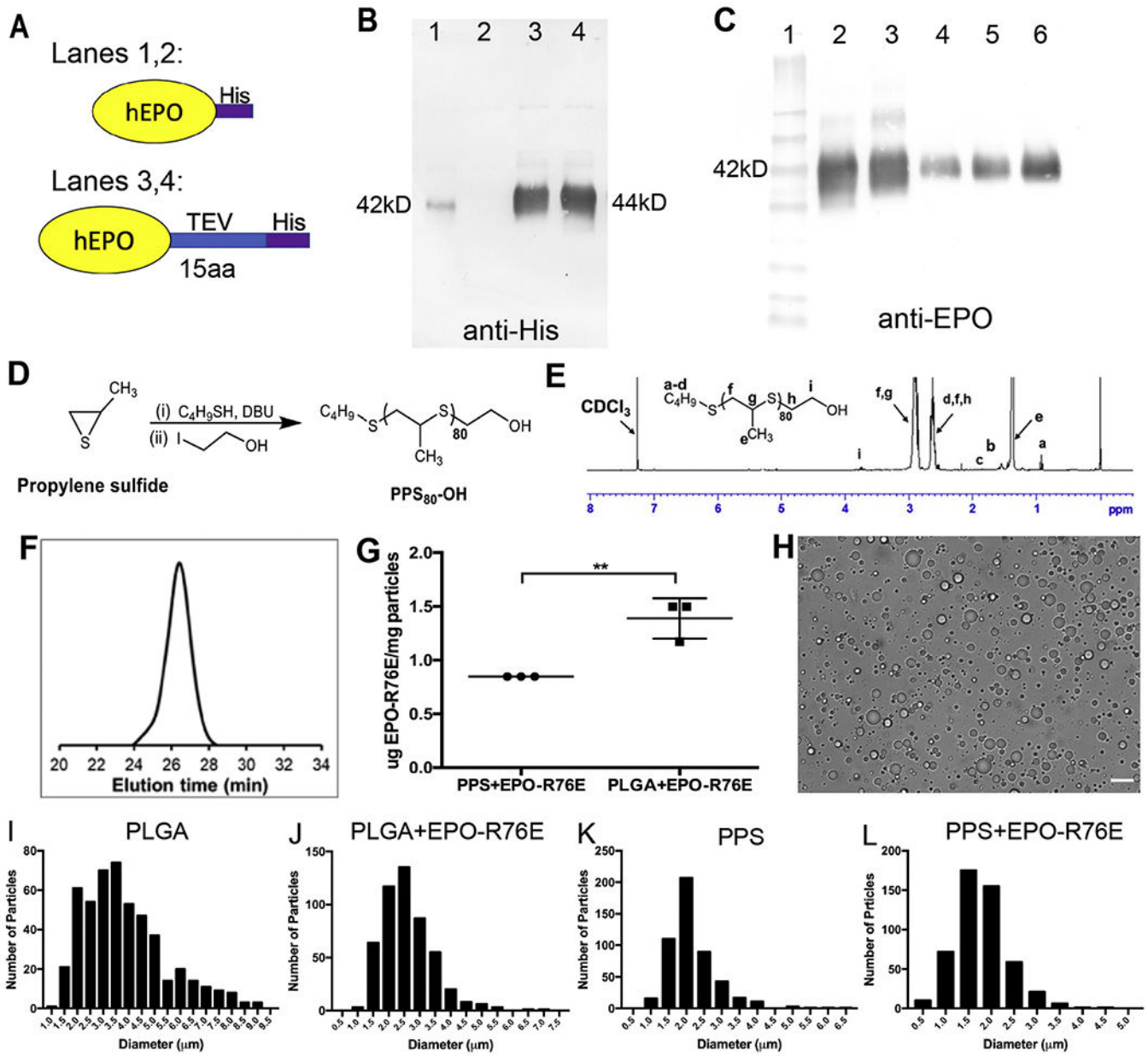

Fig. 1.

Production of EPO-R76E containing MPs. A) Schematic of two His-tagged human EPO-R76E (hEPO) that were produced. B) Detection of purified EPO-R76E using anti-His. Very little His-tagged wild-type EPO (Lane 1) and no His-tagged EPO-R76E (Lane 2) was detected. The addition of a TEV linker resulted in a large increase in the amount of detectable His-EPO (Lane 3) and His-EPO-R76E (Lane 4). Notably, both proteins are the same size. C) Detection of the TEV-His-tagged protein using anti-EPO and comparison to commercially available EPO. Lane 1: MW markers, Lane 2: wild-type EPO-TEV-His, Lane 3: EPO-R76E-TEV-His, Lanes 4–6: commercial EPO at 25 ng (4), 50 ng (5), and 100 ng (6). All were detectable with the EPO antibody and were the same size. D) Schematic for synthesis of PPS by anionic ring opening polymerization. E) ^{1}H NMR spectra of PPS in

$CDCl_3$. F) GPC refractive index detector trace of PPS (PS_{80}-OH) confirmed the formation of polymer. G) Quantification of Cy7 conjugated EPO-R76E loading into PLGA and PPS MPs. H) Representative brightfield microscopy image of unloaded PPS MPs. Scale bar represents 10 μm. I-L) Quantitative histograms demonstrating size distribution of unloaded and EPO-R76E loaded PLGA and PPS MPs. Note differences in axes between graphs.

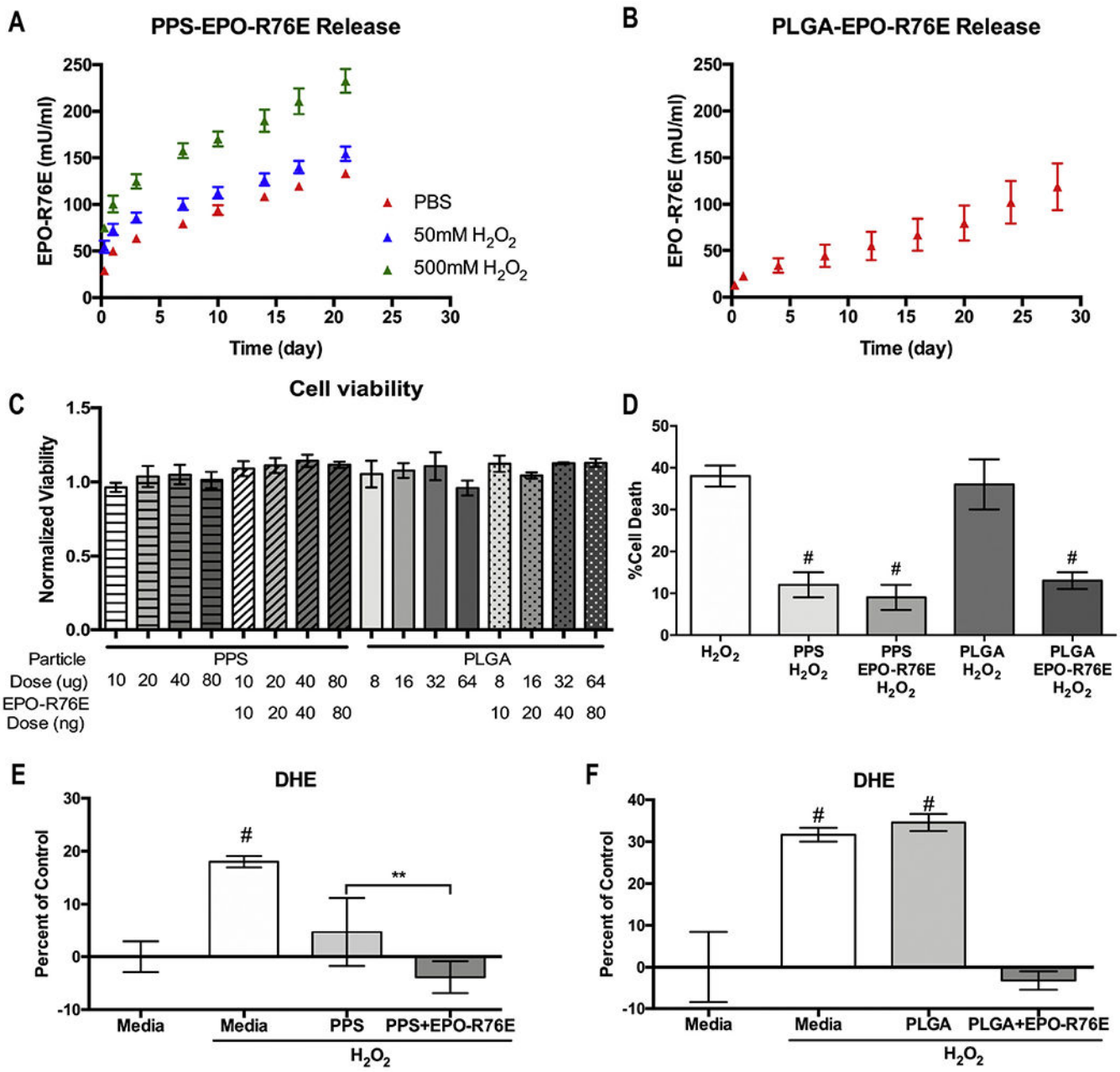

Fig. 2.

In vitro studies. A, B) Cumulative release of EPO-R76E from the PPS (A) and PLGA (B) MPs into solution over time showing mean ± s.d. C) Quantification of cell viability after exposure to different amounts of empty and loaded MPs showing mean ± s.d. D) Quantification of H_2O_2 induced ARPE-19 cell death. Cells challenged with cytotoxic levels of H_2O_2 were treated with PPS, PPS + EPO-R76E, PLGA, or PLGA+EPO-R76E MPs. E, F) Quantification of DHE fluorescence in ARPE-19 cells treated with empty or EPO-R76E loaded PPS (E) or PLGA (F) MPs. For the cell survival and DHE experiments, cells were treated with the appropriate quantity of MPs to provide a 50 ng EPO-R76E dose.

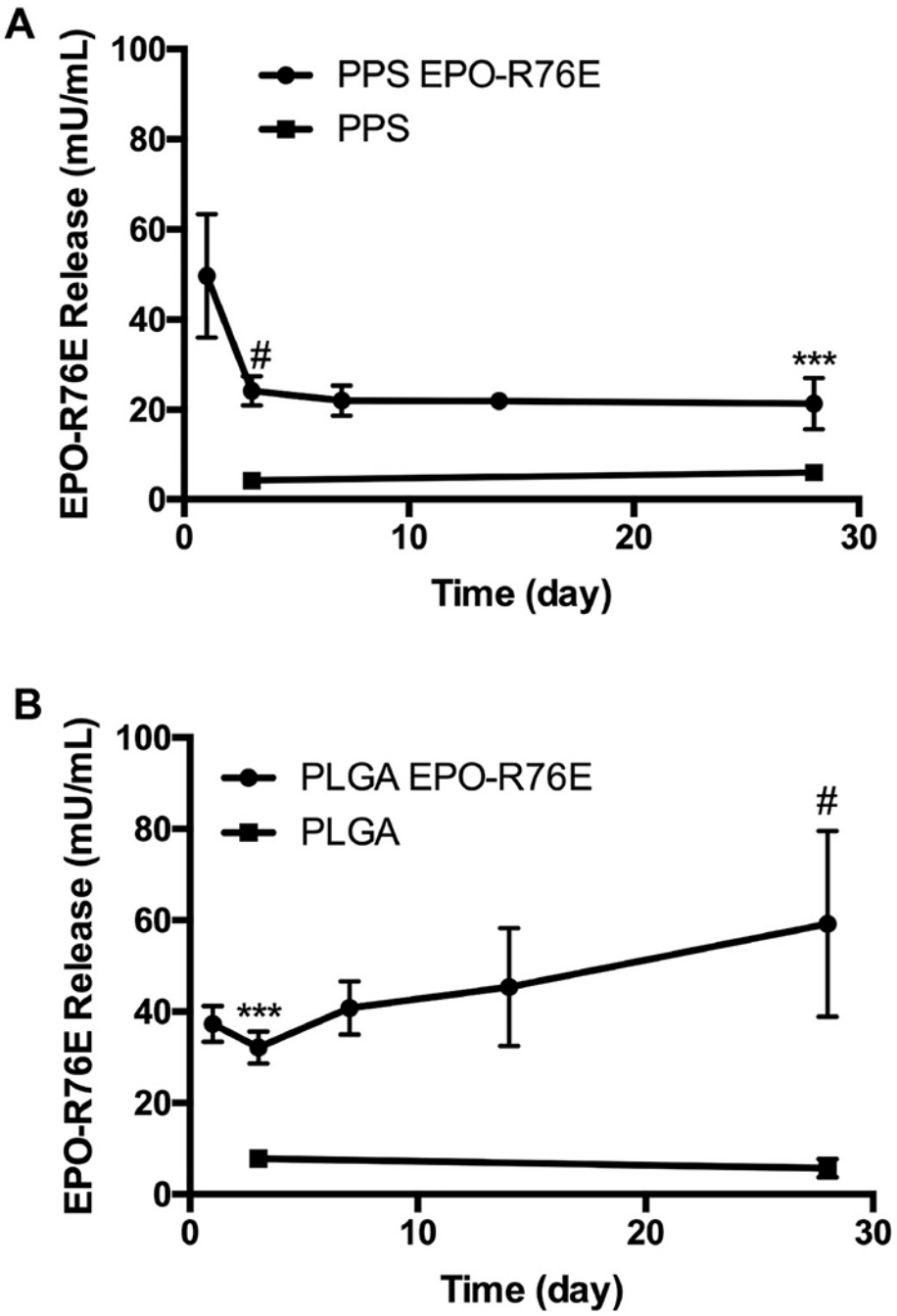

Fig. 3.

Levels of EPO-R76E in the retina at different time points after bITON and injection of empty or loaded PPS (A) or PLGA (B) MPs. Error bars = sd, ***$p < 0.001$, $^{\#}p < 0.0001$ empty compared to loaded MP-injected eyes.

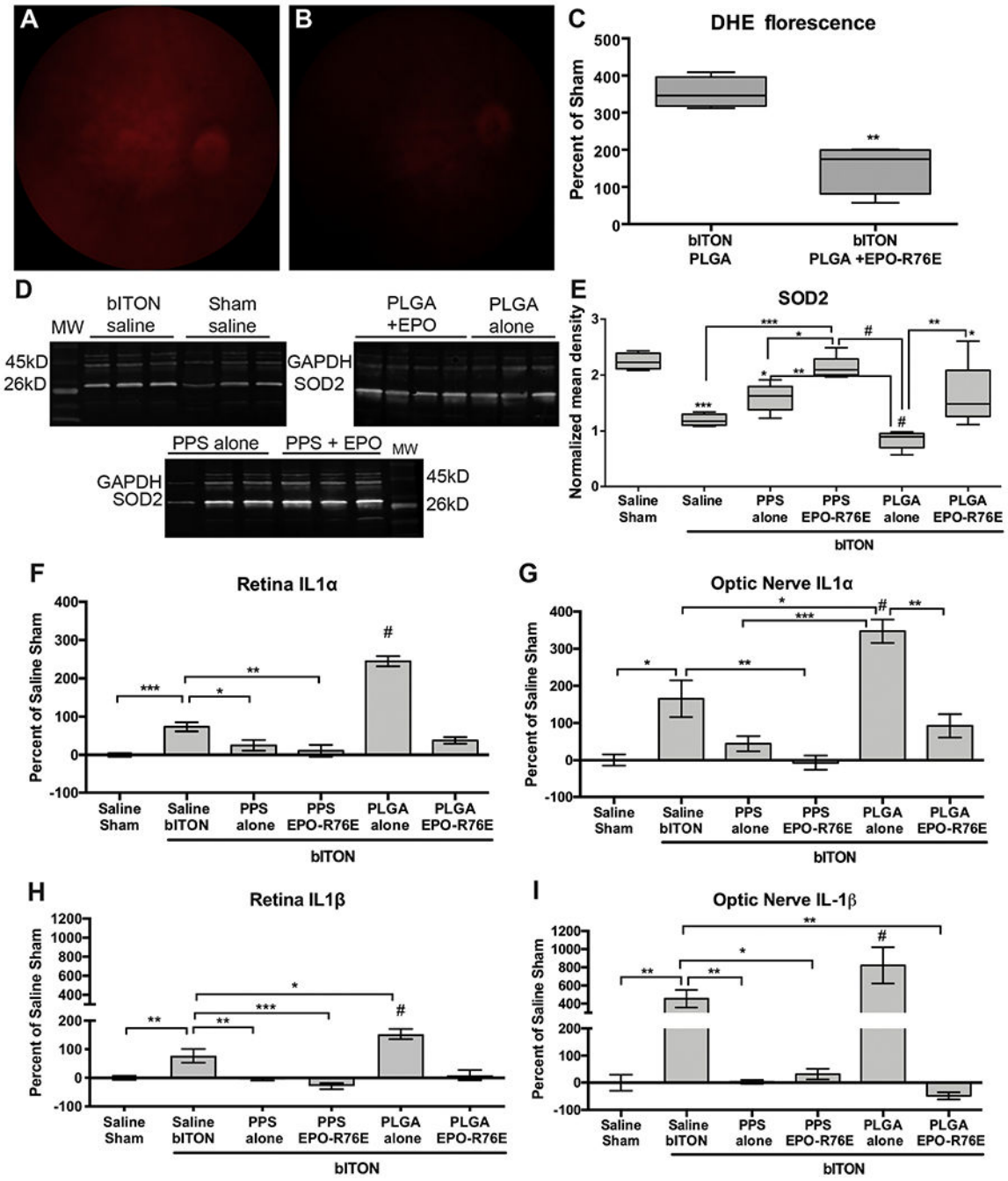

Fig. 4.

Differential effect of MPs on inflammation and oxidative stress in the retina and optic nerve. A, B) Representative fluorescence fundus images from bITON, PLGA (A) and bITON, PLGA + EPO-R76E (B) mice injected with DHE to detect superoxide and hydrogen peroxide. C) Quantification of DHE fluorescence shown as percent of sham. D) Representative western blots of SOD2 in all groups. E) Quantification of SOD2 levels after normalization to the GAPDH loading control. Statistical differences from sham are indicated without brackets. Error bars represent standard deviation. F, G) Quantification of IL-1α

levels in the retina (F) and optic nerve (G) shown as percent change relative to saline sham. Error bars represent SE. H, I) Quantification of IL-1β levels in the retina (H) and optic nerve (I) shown as percent change relative to saline sham. Error bars represent SE. *$p < 0.05$, **$p < 0.01$, ***$p < 0.001$, $^{\#}p < 0.0001$.

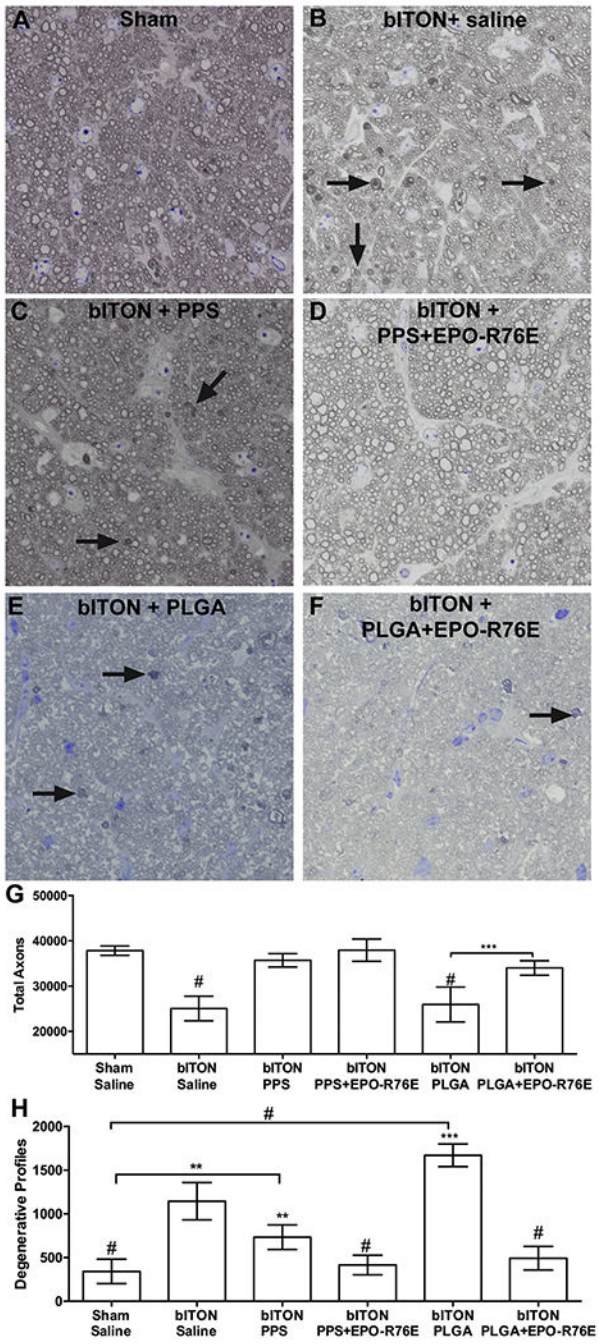

Fig. 5.

Preservation of optic nerve structure at 30-days post-injury by 1-day post-injury treatment with MPs. A-F) Brightfield micrographs of optic nerve cross-sections from sham saline (A), bITON saline (B), bITON PPS (C), bITON PPS + EPO-R76E (D), bITON PLGA (E), and bITON PLGA + EPO-R76E (F) mice. Arrows indicate degenerative axons. G) Quantification of total axons. bITON saline and bITON PLGA were different from all other groups by $p < 0.0001$. H) Quantification of degenerative axon profiles. Sham saline, bITON

PPS, bITON PPS + EPO-R76E, and bITON PLGA+EPO-R76E were all statistically different from Sham. **p < 0.01, ***p < 0.001, # p < 0.0001.

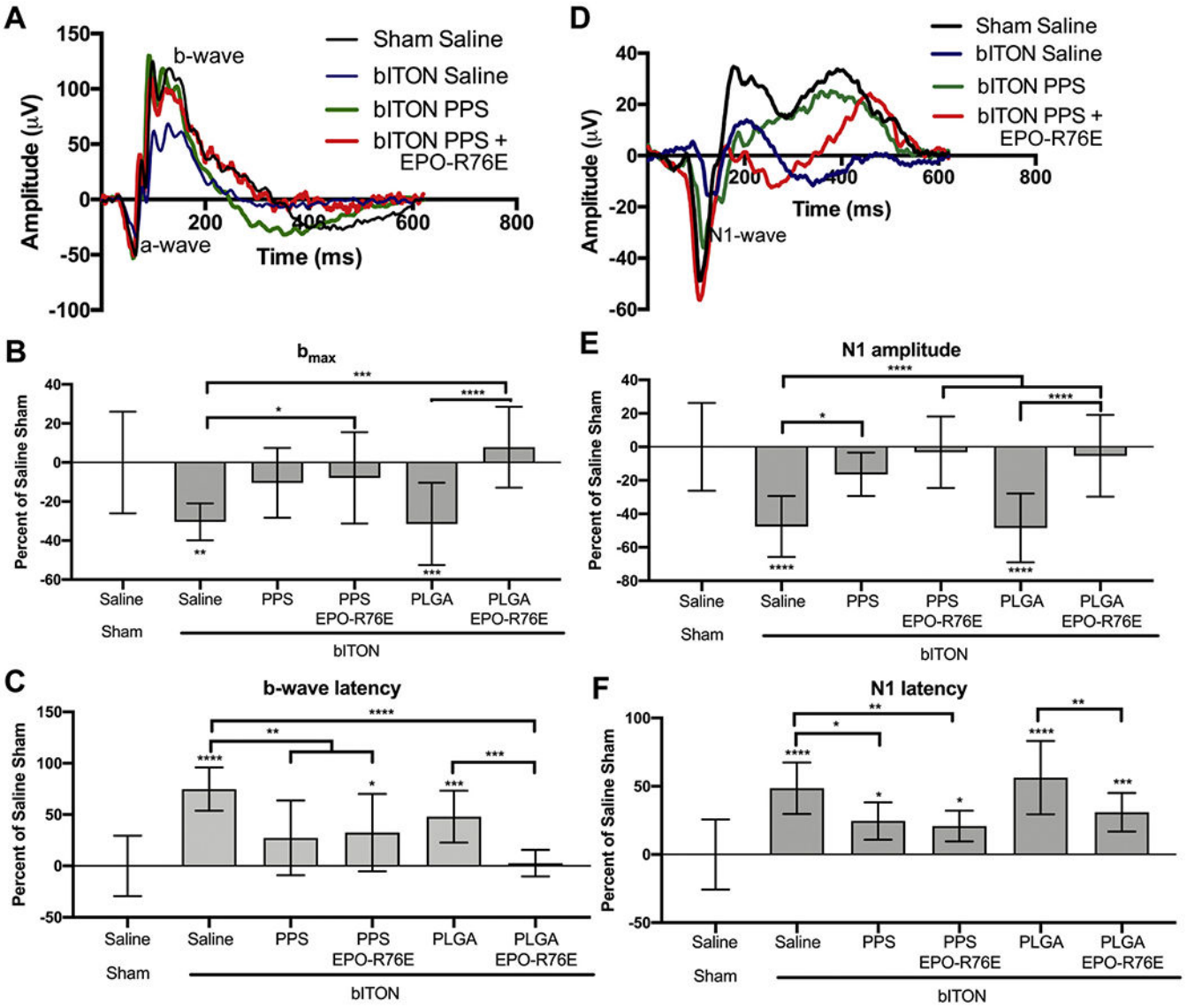

Fig. 6.

Preservation of visual function at 30-days post-injury following treatment on day 1 after injury. A) Representative ERG waveforms. B) Quantification of the b-wave amplitude. C) Quantification of the b-wave latency. D) Representative VEP waveforms. E) Quantification of the VEP N1-wave amplitude. F) Quantification of the VEP N1-wave latency. All data shown as percent change from saline sham controls. *$p < 0.05$, **$p < 0.01$, ***$p < 0.001$, $^{\#}p < 0.0001$ compared to bITON saline.

Table 1

Size quantification of MPs.

Sample	DLS (μm)	Microscopy (μm)
PLGA	4.74 ± 0.65	3.83 ± 1.6
PLGA+EPO-R76E	3.43 ± 1.18	2.60 ± 0.81
PPS	2.74 ± 0.44	2.17 ± 0.69
PPS + EPO-R76E	3.08 ± 0.97	1.78 ± 0.57